Jaqaman et al., http://www.jcb.org/cgi/content/full/jcb.200909005/DC1

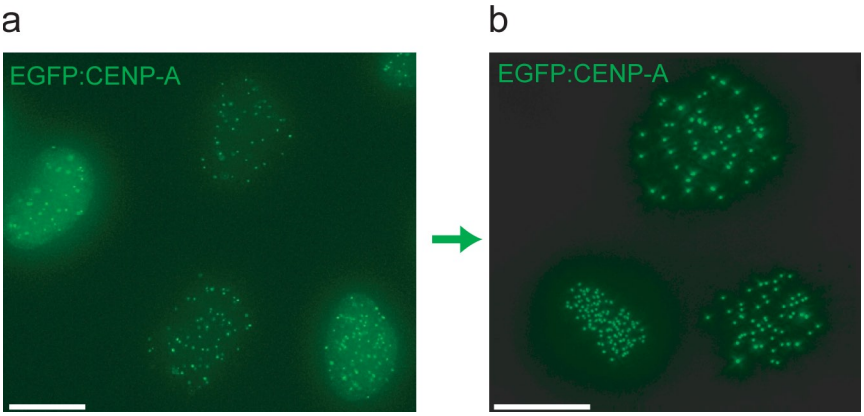

Figure S1. **Establishing a stable EGFP–CENP-A cell line.** (a) HeLa cells were transfected with pEGFP–CENP-A–IRESpuro, and positive colonies were selected in puromycin. (b) A second round of clonal selection yielded a population with homogeneous kinetochore signal intensity. Bars, 10 µm.

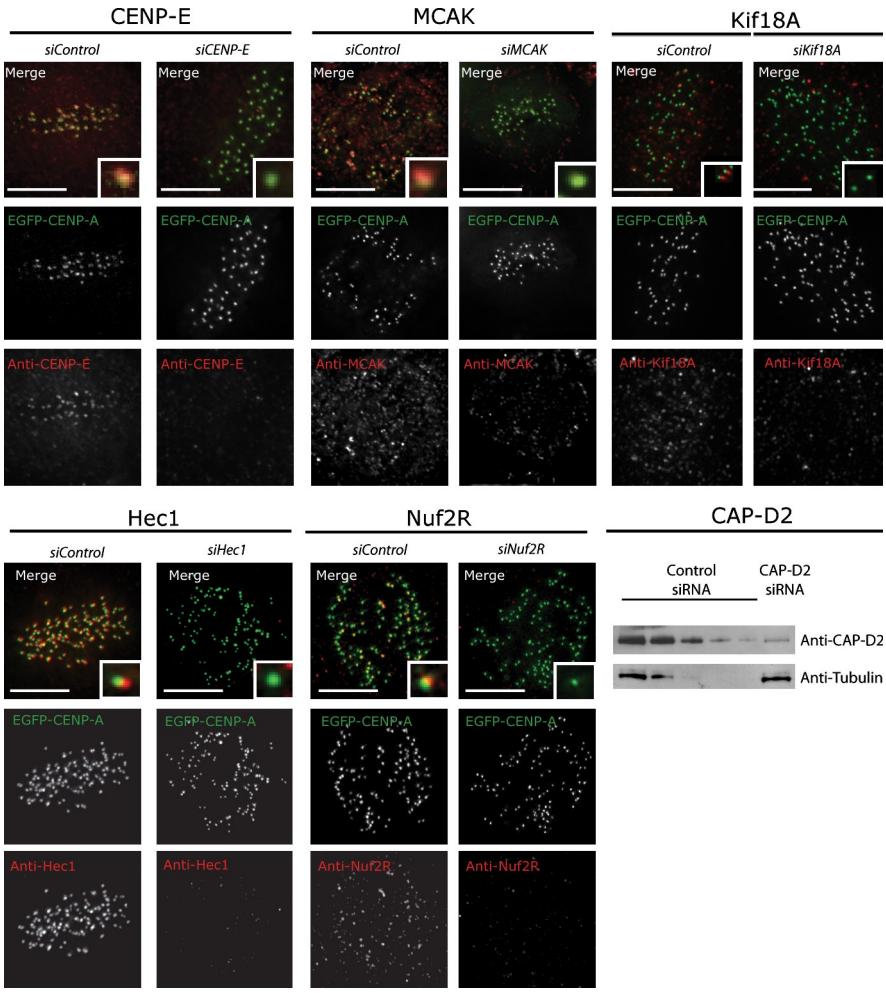

Figure S2. **Confirmation of kinetochore protein depletions by siRNA.** Representative immunofluorescence images of mitotic EGFP–CENP-A cells transfected with siRNA oligonucleotides as indicated and stained with antibodies raised against the kinetochore protein targeted for deletion (red). EGFP–CENP-A (green) marks the position of kinetochores. CAP-D2 expression was validated by Western blot analysis. Inset images (top) show magnifications of a single sister kinetochore. Bars, 5 µm.

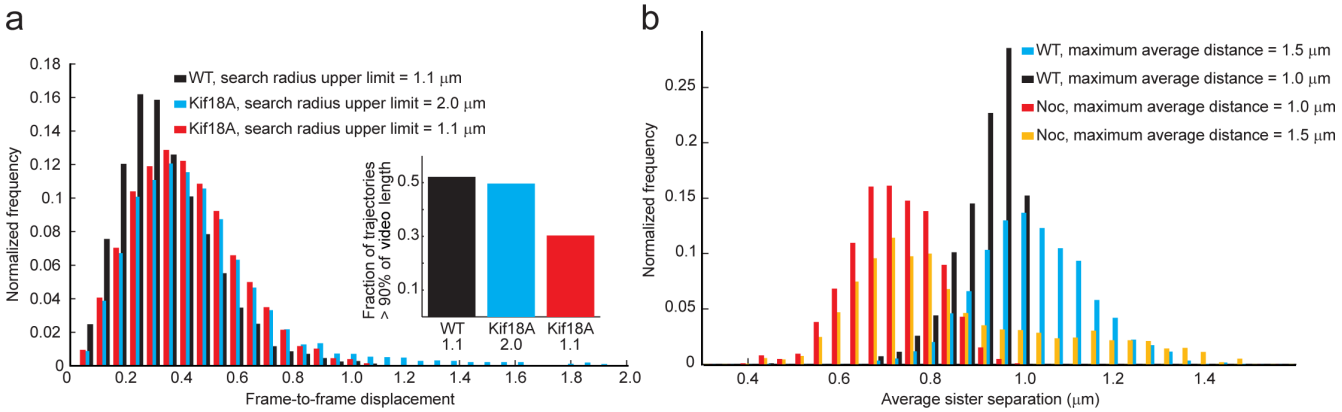

Figure S3. **Critical image analysis parameters were varied to obtain results of similar quality.** (a) Tracking search radius upper limit was varied to obtain tracks of similar quality. Frame to frame kinetochore displacement histograms resulting from tracking WT cells with the proper search radius upper limit of 1.1 μm (black), tracking Kif18A-depleted cells with the proper, expanded search radius upper limit of 2 μm (cyan), and tracking Kif18A-depleted cells with a search radius upper limit of 1.1 μm as used for WT (red). The larger displacements captured by tracking Kif18A-depleted cells with an expanded search radius upper limit are necessary to obtain tracks of similar quality to WT, as judged by the fraction of trajectories spanning >90% of the video in both cases (inset). (b) Maximum average distance for trajectory pairing was varied to obtain sister pairs of similar quality. For trajectory pairing in WT and nocodazole (noc)-treated cells, the optimal maximum average distance was 1.5 and 1 μm, respectively, yielding smoothly decaying and symmetric average sister separation distributions (cyan and red). If a maximum average distance of 1 μm was imposed on WT cells, the resulting average sister separation distribution was abruptly terminated (black), indicating that many sisters were lost as a result of the too-stringent pairing criterion. However, if a maximum average distance of 1.5 μm was used for nocodazole, the resulting average sister separation distribution had a long tail at large sister separations (yellow), which is indicative of erroneous trajectory pairings.

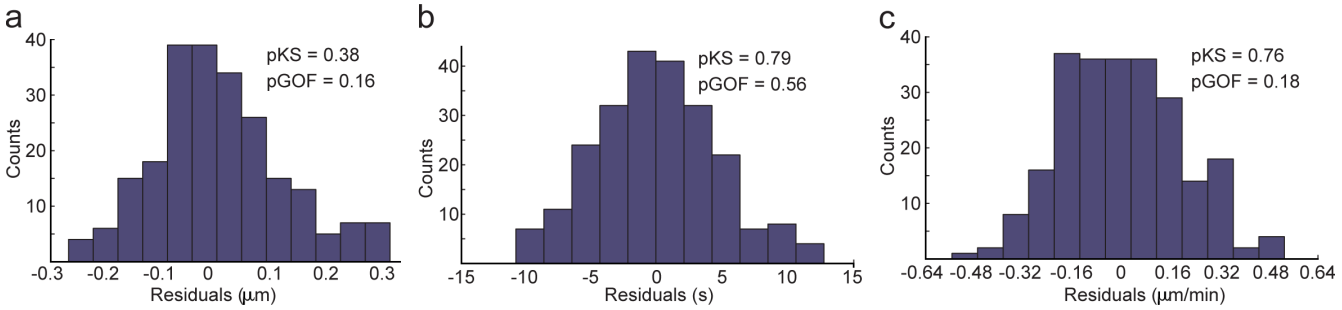

Figure S4. **The relationship of oscillation extent, oscillation half-period, and center normal speed to plate thickness can be modeled as linear.** (a–c) The distribution of residuals from fitting WT oscillation extent (a), oscillation half-period (b), and center normal speed (c) versus plate thickness with a straight line using least-median squares. All distributions are close to normal, as indicated by the p-value of the Kolmogorov–Smirnov test, comparing them to a normal distribution (pKS > 0.1). All fits also pass the χ^2 goodness of fit test (pGOF > 0.1), implying that a straight line is sufficient to describe the relationship between plate thickness and the three variables.

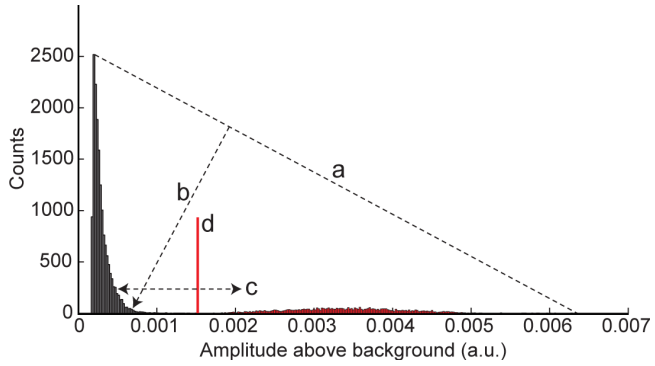

Figure S5. **Automatic thresholding of amplitude histogram to distinguish kinetochores signals from noise.** The algorithm was based on that developed by Rosin (2001) and consisted of four steps. (a) A straight line was drawn between the histogram peak and the first empty bin after the largest amplitude. (b) The Rosin threshold was defined as the bin i with counts H_i such that the point (i, H_i) was furthest away from the straight line defined in a. (c) To increase the accuracy and robustness of the thresholding, one minimum to the left of the Rosin threshold and two minima to its right were located. (d) The final threshold was defined as the deepest of the three minima, with kinetochore signals above the threshold (red) and noise signals below it (black).

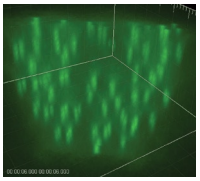

Video 1. **Time-lapse sequence of an unperturbed (WT) EGFP–CENP-A HeLa cell in late prometaphase.** The signal of each kinetochore is ellipsoidal, reflecting the shape of the PSF in 3D, where it is longer in the axial direction than in the lateral direction. Video consists of 41 time points comprised of 20 z sections 0.5 µm apart acquired every 7.5 s for 5 min. Grid spacing is 2 µm in all directions.

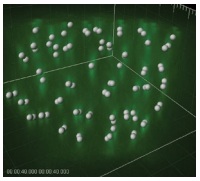

Video 2. **Detection of EGFP–CENP-A signals in the time-lapse sequence of Video 1.** Each sphere represents a detected kinetochore and is centered at the estimated position of that kinetochore (i.e., the centroid of the ellipsoidal signal of the kinetochore). The size of the spheres is arbitrary, but it is the same for all kinetochores. The signal of each kinetochore is ellipsoidal, reflecting the shape of the PSF in 3D, where it is longer in the axial direction than in the lateral direction. Video consists of 41 time points comprised of 20 z sections 0.5 µm apart acquired every 7.5 s for 5 min. Grid spacing is 2 µm in all directions.

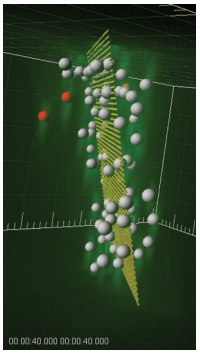

Video 3. **Plane fit through aligned kinetochores and identification of unaligned kinetochores in the time-lapse sequence of Video 1.** For clarity, the viewing angle in this video is different from the Videos 1, 2, 4, and 5. Yellow plane, plane fit; white spheres, kinetochores; red spheres, unaligned kinetochores. The signal of each kinetochore is ellipsoidal, reflecting the shape of the PSF in 3D, where it is longer in the axial direction than in the lateral direction. Video consists of 41 time points comprised of 20 z sections 0.5 µm apart acquired every 7.5 s for 5 min. Grid spacing is 2 µm in all directions.

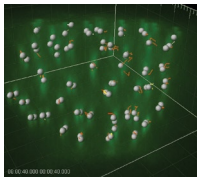

Video 4. **Tracking of detected kinetochores in the time-lapse sequence of Video 1.** Drag tails show tracks in a four-frame rolling window: red, tracks that last for ≥90% of video length; blue, tracks that last for <90% but ≥50% of video length; yellow, tracks that last for <50% of video length. Smaller spheres (e.g., in the bottom left corner in frames 10–12) are placeholders for kinetochores whose detection temporarily failed but whose tracks were rescued by gap closing (Jaqaman et al., 2008). The signal of each kinetochore is ellipsoidal, reflecting the shape of the PSF in 3D, where it is longer in the axial direction than in the lateral direction. Video consists of 41 time points comprised of 20 z sections 0.5 µm apart acquired every 7.5 s for 5 min. Grid spacing is 2 µm in all directions.

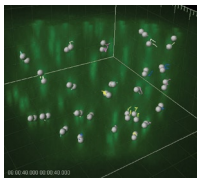

Video 5. **Identification of sister kinetochore pairs in the time-lapse sequence of Video 1.** Drag tails show tracks in a four-frame rolling window. Sister pairs are color coded for clarity (the plotting algorithm rotated through six colors). Smaller spheres (e.g., in the bottom left corner in frames 10–12) are placeholders for sisters that were temporarily lost because of the temporary failure to detect one or both sister kinetochores. Sister pairing is sensitive to all previous image analysis steps, and is thus a good measure of the overall quality of image analysis. The signal of each kinetochore is ellipsoidal, reflecting the shape of the PSF in 3D, where it is longer in the axial direction than in the lateral direction. Video consists of 41 time points comprised of 20 z sections 0.5 µm apart acquired every 7.5 s for 5 min. Grid spacing is 2 µm in all directions.

Table S1. **siRNA oligo sequences and primary antibody sources and dilutions**

siRNA/antibody	siRNA sequence reference	Antibody reference	Antibody dilution
Hec1	Meraldi et al., 2004	GeneTex	1:2,000
Nuf2R	Meraldi et al., 2004	Meraldi et al., 2004	1:500
MCAK	Cassimeris and Morabito, 2004	Cytoskeleton, Inc.; Toso et al., 2009	1:1,000
KIF18A	Stumpff et al., 2008	Stumpff et al., 2008	1:250
CENP-E	Martin-Lluesma et al., 2002	Meraldi and Sorger, 2005	1:1,500
CAP-D2	Hirota et al., 2004	Kimura et al., 2001	1:1,000
Separase	Tang et al., 2004	NA	NA

NA, not applicable.

Table S2. **Number of imaged cells and sister pairs used for analysis**

Conditions	Number of cells	Sister pairs	Number of sister pairs/cell
With metaphase plate			
WT	212	6,605	31.2
WT synchronized	33	1,142	34.6
Taxol[a]	29	520	17.9
Fixed	10	400	40.0
siMCAK	72	2,884	40.1
siKif18A	23	621	27.0
siCENP-E	66	1,826	26.6
siCAP-D2	32	703	22.0
siSeparase	40	1,431	35.8
Without metaphase plate			
Nocodazole	34	1,259	37.0
siHec1 synchronized	17	584	34.4
siNuf2R synchronized	18	587	32.6
siCENP-E + taxol	72	2,345	32.6

For conditions with a metaphase plate, the reported number of sister pairs refers to aligned sisters only.

[a]Number of aligned sister pairs is low after taxol treatment because many sister pairs do not congress to the metaphase plate, although there are enough aligned sisters to identify a plate.

Table S3. **Parameters, their default values, and exceptions**

Parameter	Default	Exceptions
Adjustable tracking parameters		
Gap-closing time window	Four frames	None
Search radius upper limit- aligned (µm)	1.1	*siKif18A* (2.0) *siHec1*[a], *siNuf2R*[a] (2.0)
Search radius upper limit- unaligned (µm)	3.0	None
Adjustable sister pairing parameters		
Maximum average distance (µm)	1.5	Nocodazole (1.0) Taxol, *siCENP-E* + taxol (1.2) *siHec1*, *siNuf2R* (1.3) *siCAP-D2* (1.9)
Maximum average angle with normal (°)	30	*siKif18A* (45)

[a]Conditions without metaphase plate, thus no aligned versus unaligned kinetochore classification. Therefore, all kinetochores get the same tracking parameters.

References

Cassimeris, L., and J. Morabito. 2004. TOGp, the human homolog of XMAP215/Dis1, is required for centrosome integrity, spindle pole organization, and bipolar spindle assembly. *Mol. Biol. Cell.* 15:1580–1590. doi:10.1091/mbc.E03-07-0544

Hirota, T., D. Gerlich, B. Koch, J. Ellenberg, and J.M. Peters. 2004. Distinct functions of condensin I and II in mitotic chromosome assembly. *J. Cell Sci.* 117:6435–6445. doi:10.1242/jcs.01604

Jaqaman, K., D. Loerke, M. Mettlen, H. Kuwata, S. Grinstein, S.L. Schmid, and G. Danuser. 2008. Robust single-particle tracking in live-cell time-lapse sequences. *Nat. Methods.* 5:695–702. doi:10.1038/nmeth.1237

Kimura, K., O. Cuvier, and T. Hirano. 2001. Chromosome condensation by a human condensin complex in *Xenopus* egg extracts. *J. Biol. Chem.* 276:5417–5420. doi:10.1074/jbc.C000873200

Martin-Lluesma, S., V.M. Stucke, and E.A. Nigg. 2002. Role of Hec1 in spindle checkpoint signaling and kinetochore recruitment of Mad1/Mad2. *Science.* 297:2267–2270. doi:10.1126/science.1075596

Meraldi, P., V.M. Draviam, and P.K. Sorger. 2004. Timing and checkpoints in the regulation of mitotic progression. *Dev. Cell.* 7:45–60. doi:10.1016/j.devcel.2004.06.006

Meraldi, P., and P.K. Sorger. 2005. A dual role for Bub1 in the spindle checkpoint and chromosome congression. *EMBO J.* 24:1621–1633. doi:10.1038/sj.emboj.7600641

Rosin, P.L. 2001. Unimodal thresholding. *Patt. Recogn.* 34:2083–2096. doi:10.1016/S0031-3203(00)00136-9

Stumpff, J., G. von Dassow, M. Wagenbach, C. Asbury, and L. Wordeman. 2008. The kinesin-8 motor Kif18A suppresses kinetochore movements to control mitotic chromosome alignment. *Dev. Cell.* 14:252–262. doi:10.1016/j.devcel.2007.11.014

Tang, Z., Y. Sun, S.E. Harley, H. Zou, and H. Yu. 2004. Human Bub1 protects centromeric sister-chromatid cohesion through Shugoshin during mitosis. *Proc. Natl. Acad. Sci. USA.* 101:18012–18017. doi:10.1073/pnas.0408600102

Toso, A., J.R. Winter, A.J. Garrod, A.C. Amaro, P. Meraldi, and A.D. McAinsh. 2009. Kinetochore-generated pushing forces separate centrosomes during bipolar spindle assembly. *J. Cell Biol.* 184:365–372. doi:10.1083/jcb.200809055